Desalination and Water Treatment
www.deswater.com

doi: 10.5004/dwt.2023.29468

291 (2023) 92–100
April

Effect of bubble diameter and bubble count on overall mass transfer coefficient using ImageJ analysis in a down flow jet loop sparged reactor

G. Mugaishudeen*, R. Ashwin, A.R. Arthanarieaswaran, K. Jeevitha

Department of Chemical Engineering, Kongu Engineering College, Perundurai, Tamil Nadu, India, email: mugais.chem@kongu.edu (G. Mugaishudeen), ashwingeeaar@gmail.com (R. Ashwin), ganukarthi3@gmail.com (A.R. Arthanarieaswaran), jeevithaksmj@gmail.com (K. Jeevitha)

Received 26 April 2022; Accepted 18 March 2023

ABSTRACT

Bubble size and bubble count play a vital role while determining the overall mass transfer coefficient of a jet loop reactor. A self-designed down flow jet loop sparged reactor with an air–water system was investigated for bubble size and bubble count. The influence of parameters such as liquid flow rate (Q_L), gas flow rate (Q_G), number of sparger openings, and sparger diameter was studied in detail. Among the various operating conditions, the maximum overall mass transfer coefficient was found to be at a 27 cm projection depth of the ejector with 4 sparger openings and a diameter of 2 mm. The bubble pictures were taken in a good quality digital single-lens reflex with 50× zoom. The captured images were analyzed using ImageJ analysis. The results showed that the bubble count increased with increasing flow rates of gas and liquid whereas the bubble diameter decreased with increasing gas and liquid flow rates.

Keywords: Jet loop reactor; Down flow; Overall mass transfer coefficient; Bubble diameter; Bubble count; Gas holdup; Perforated sparger

1. Introduction

Many chemical and biochemical processes such as petroleum refining, hydrogenation, fermentation, and wastewater treatment which involves gas–liquid reactions are carried out in different types of reactors, for example, continuous stirred-tank reactors, bubble column sparged vessels, and the recently developed loop reactors. Loop reactors are characterized by a well-defined flow regime, better distribution effects, and high mass transfer performance compared to conventional reactors. The down flow jet loop reactor is a novel design, which has attracted considerable interest in recent years for its application in gas–liquid and gas–liquid–solid reactions. Loop reactors are cylindrical or rectangular vessels (L/D > 1), in which multiphase fluid either by means of a liquid jet or as a result of difference in density and was subsequently circulated around a draft tube (internal loop) or by an external tube (external loop) and dispersion of gas phase is achieved by means of a jet or static dispersion device. Most of the investigations conducted on jet loop reactors were with a central draft tube and two fluid nozzle placed at the bottom of the reactor [1–3]. This type of reactor was distinguished by jet or nozzle in which the liquid jet enters the reactor through the nozzle, which is the middle of a gas jet. The liquid jet takes responsibility of distribution and dispersion of the gas as fine bubbles in the liquid and also in the circulation of gas–liquid concoction by momentum transfer [4]. However, the use of such a nozzle had an adverse effect on the two-phase gas circulation because the gas forms an envelope around the liquid jet as a result of the increase in the volumetric gas flow rate. When this arrangement was implemented in a slurry reactor and in processes involving varyingly soluble gas, as the result of a blockage in the nozzle and minimum residence time of the gas particles, this arrangement was considered to have drawbacks.

* Corresponding author.

Thus as an alternative gas phase was launched at the top of jet propelled loop reactor, here the liquid leaving the nozzle forms a hollow cone with inner and outer momentum transfer areas [5,6]. With such an arrangement, the primary dispersion of gas and circulation of the reactor fluid can be controlled independently. The gas–liquid contactor with ejector type distributor exhibits favorable features including most notably self-sucking and efficient dispersion of gas phase resulting in large values of overall mass transfer coefficient. when we use venturi ejectors in reactor for air–water system, internal circulation and turbulence in the main holding tank, as well as the external circulation of the dispersion were found to be low when compared with straight throat ejector [7]. Secondary dispersion in the main tank was less uniform. In addition, the opposing buoyancy force of the gas bubbles resulted in relatively low internal and external circulation of the dispersion. When venturi ejectors are used in the reactor to handle electrolytic aqueous solution, the bubble sizes were much smaller because of shrinkage and breakage of primary bubbles at the exit of the throat.

The gas holdup and number of bubbles is directly related to the operational variables, such as the gas and liquid flow rates. The higher the gas holdup, the more would be the interfacial area and thereby increasing the transfer of gas to the liquid. Whereas the bubble diameter is inversely proportional to the gas and liquid flow rates [8,9]. Baffles are used due to the lower gas holdup in bubble column reactor caused by the higher liquid circulation velocity and the bubble coalescence in the draft tube [16]. The placement of baffles inside the reactor would increase the mean residence time in the jet loop reactor. The mean residence time refers to the time spent by the molecule inside the reactor. The gas phase residence time can be increased considerably in down flow reactor when the gas is introduced from the top of the liquid flowing co-currently downwards, so that bubbles were found to move in a direction opposite to their buoyancy. Also the introduction of sparger at the bottom end of the ejector will enhance the dispersion rate by creating finer uniform bubbles. So the straight throat ejector with sparger has been selected for air-water system in which interfacial mass transfer is the rate-controlling step. The overall production rate of chemical processes often is limited by gas–liquid mass transfer. So the study of mass transfer coefficient is essential for the design of reactors. From the previous work it can be noted that the studies available in the literature on overall mass transfer performance in down flow jet loop reactor with straight throat ejector type gas distributor are limited. Also no one has reported the effect of bubble size and bubble count on overall mass transfer coefficient in down flow jet loop reactor. Experiments were conducted in down flow jet loop sparged reactor to understand the influence of gas and liquid flow rate, sparger diameter, and sparger openings on bubble size and bubble count and so as the overall mass transfer coefficient.

2. Experimental set-up

The provisional setup of the experiment is shown in Fig. 1. The jet loop reactor consists of two sections, top straight throat ejector and middle cylindrical reactor section. The ejector is nothing but a straight galvanized iron (GI) pipe of 2.6 cm inner diameter with air entry on top. In the ejector water enters perpendicular to that of air as shown in Fig. 2. The reactor comprises a vertical Perspex tube with a hemispherical bottom. The effectiveness of the down flow jet loop reactor significantly relies on the design of the sparger. It has a significant impact on the dispersion of gas in the liquid phase by creating resistance to the flow and thereby increasing the velocity. The perforated sparger geometry used in our study is shown in Fig. 3. The sparger is introduced at the bottom end of the straight throat ejector and placed coaxially inside the baffle plates. Non-circular baffle plates were set 0.07 m above the bottom of the column by the use of flanges as shown in Fig. 4. The gas and the liquid phases enter at the top of the straight throat ejector and flow co-currently towards the bottom. The sparger disperses the gas phase in the liquid phase leading to fine and uniform bubble formation. The bubbles due to their high velocity

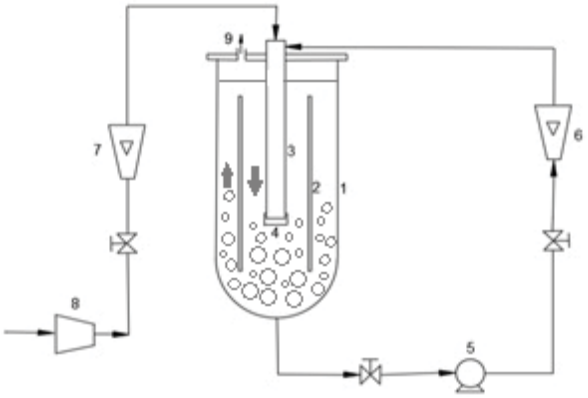

Fig. 1. Schematic representation of the down flow jet loop reactor, 1. Reactor; 2. Non-circular baffle plates; 3. Straight throat ejector; 4. sparger; 5. Pump; 6. Liquid flow rotameter; 7. Gas flow rotameter; 8. Compressor; 9. Gas vent.

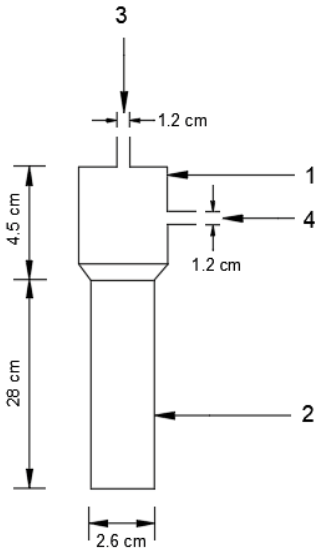

Fig. 2. Configuration of straight throat ejector, 1. Injector chamber; 2. Straight diffuser throat; 3. Air inlet; 4. Water inlet.

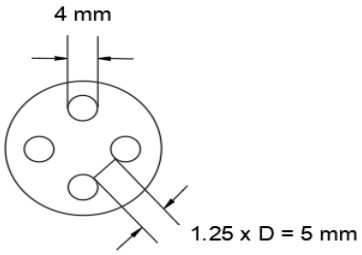

Fig. 3. Perforated sparger geometry with four openings.

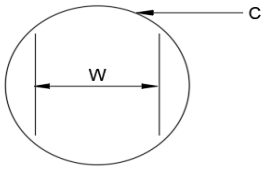

Fig. 4. Shape of non-circular baffle plate C = reactor column; W = Distance between two non-circular baffles.

imparted from the motive fluid travel downwards along the baffles and reach the top of the reactor. This forms an internal loop within the reactor. The liquid is withdrawn at the bottom of the reactor with the help of a pump and recycled back to the straight throat ejector through a liquid flow meter. This forms the external loop. The air is sent to the top of the reactor through a gas flow meter by the compressor. The experiment is studied at room temperature (25°C–28°C) and tap water is used as the liquid phase. The dimensions of the experimental set-up are given in Table 1.

3. Materials and methods

In our study, we used air and tap water as gas and liquid phases, respectively. The flow rate of air was measured at the ambient temperature and atmospheric pressure. The overall gas holdup (ε_G) in the reactor was determined in our studies. The technique used here is volume expansion technique. During steady state operation, by adjusting the solenoid valves the air and liquid flow is stopped and ε_G was estimated by the ratio of the difference between the height of two-phase dispersion (H_F) and the height of clear liquid (H_L) to the two-phase dispersion height (H_F) using the following equation [7–10].

$$\varepsilon_G = \frac{\left(H_F - H_L\right)}{H_F}$$

The transient gassing-in (gassing-out) process was used for the calculation of overall volumetric mass transfer coefficient (k_La). A volume of liquid slightly greater than that of reactor and pipelines was taken in the cylindrical column. By closing the ejector, the gas flow rate was stopped with suitable enclosure. Then the oxygen concentration in the liquid was made approximately zero in a few minutes by rapid addition of 160 mg/L of sodium sulphite ($Na_2SO_3{\cdot}7H_2O$) in addition with 2 mg/L of cobaltous chloride ($COC1_2{\cdot}6H_2O$) as a catalyst. By opening the enclosure of the ejector tube air flow to the reactor was initiated and change in time with respect to the oxygen concentration was monitored by a dissolved oxygen electrode (Hanna HI98193).

Table 1
Dimensions of the downflow jet loop reactor

Reactor inner diameter (D_R)	14.2 cm
Reactor height (H_R)	60 cm
Nozzle inner diameter (D_Z)	1.2 cm
Baffle plate length (L_B)	35 cm
Baffle plate thickness (T_B)	0.1 cm
Baffle plate width (W_B)	12 cm
Sparger opening diameters (D_S)	2, 3, 4 mm
No of sparger opening (N_S)	4
Gas flow rate (Q_G)	5–12.5 L/min
Liquid flow rate (Q_L)	5–12.5 L/min

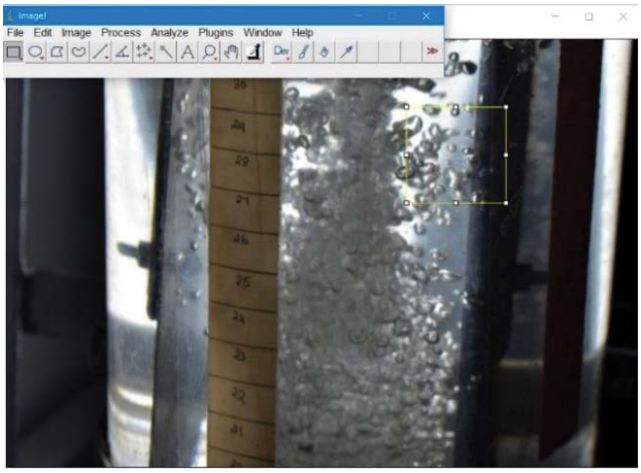

Fig. 5. Step 1: Selection of captured bubbles.

The constant gas phase composition with reference to axial position in the reactor, well mixed transfer time ($1/k_La$) for the entire range of liquid velocity covered was taken as assumption. Since the state of $k_La < 1/\tau_E$ was attained, the influence of oxygen dynamics of electrode was neglected in the estimation and the values of k_La for each run was obtained from the slope of the straight line in the plot $\ln[(C^*–C_0)/(C^*–C)]$ vs. time. The steady state value of dissolved oxygen meter at favorable operating conditions of liquid flow rates was noted as the saturation or equilibrium concentration (C^*) of oxygen, initial concentration of oxygen (C_0) and concentration of oxygen at time (C) in the liquid for that particular experimental run [11].

3.1. Bubble geometry studies using ImageJ

The bubble diameter and number of bubbles is determined by capturing the bubble images in a good quality digital single-lens reflex with 50× zoom. The background lighting should be avoided for better results during the image analysis. The greater the picture quality greater will be the

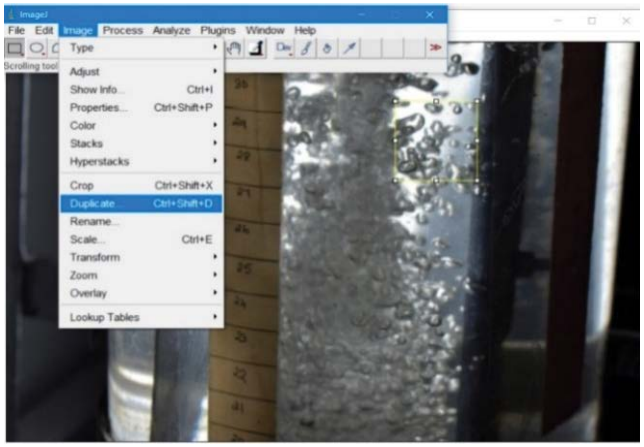

Fig. 6. Step 2: Selection of region for bubble analysis.

Fig. 7. Step 3: Conversion of selected region to threshold (8-bit).

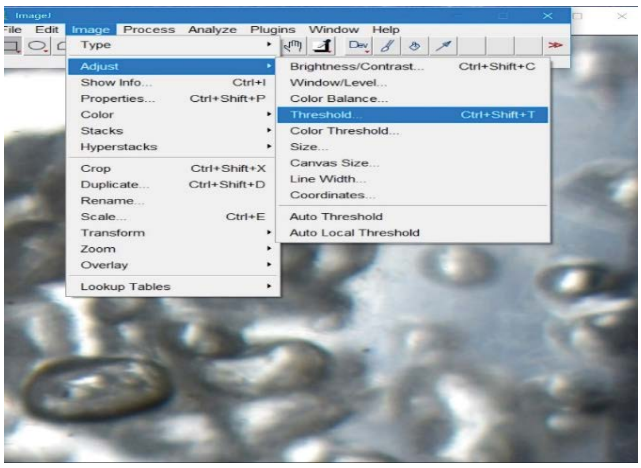

Fig. 8. Step 4: Adjustment of threshold level of the region.

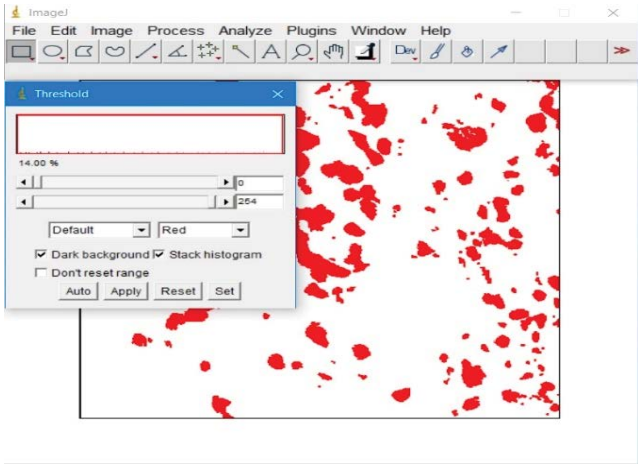

Fig. 9. Step 5: Adjustment of threshold level of the region with only bubbles.

results of the ImageJ analysis. ImageJ is public domain software using java image processing technology. The captured pictures were converted into gray scale (8 bit) for analysis. The proper image section without any background disturbances and with clean section of bubbles were cropped and duplicated in ImageJ. The threshold level of the photo was adjusted so that the clear and full cross section of the bubble image is selected. Then the image is analyzed for bubble count and bubble diameter [23–27]. The calculated values for the specific area is multiplied to the total area of the reactor cross section. The screen snips during the evaluation of bubble count are displayed as shown in Figs. 5–11.

4. Results and discussion

4.1. Effect of gas flow rate

The experiment was done by varying the gas flow rate at constant liquid flow rate. The influence of gas flow rate on bubble diameter and bubble count was studied. As the flow rate increases the number of bubbles also increases in accordance with velocity and the bubble diameter decreases. As shown in Figs. 12 and 13 results are found to be increased gas entrainment and gas–liquid interfacial area at higher gas flow rates. Similar trends have been reported in the literature for various configurations of jet loop reactors [6–8]. Figs. 16–19 show the bubble analysis (grey scale and threshold view) done using ImageJ software to find the average bubble diameter and approximate bubble count [28–30].

4.2. Overall mass transfer coefficient and gas holdup variation with sparger geometry

According to Henry's Law, the increased pressure from the sparger allows greater dissolution of gases into the water, only occurs in the chemical reaction between liquid and gas under equilibrium (saturated). Higher the k_La value, faster the mass transfer rate. Among the other 3 mm and 4 mm spargers, the 2 mm sparger produced the largest k_La of 1.402 min^{-1} as shown in Figs. 13 and 15 at a projection depth of 27 cm and gas flow rate of 12.5 L/min. While the 3 mm sparger and 4 mm sparger produced 1.401 and 1.35 min^{-1}, respectively. The main factors influenced the increasing k_La produced by each sparger were the size of the bubbles with

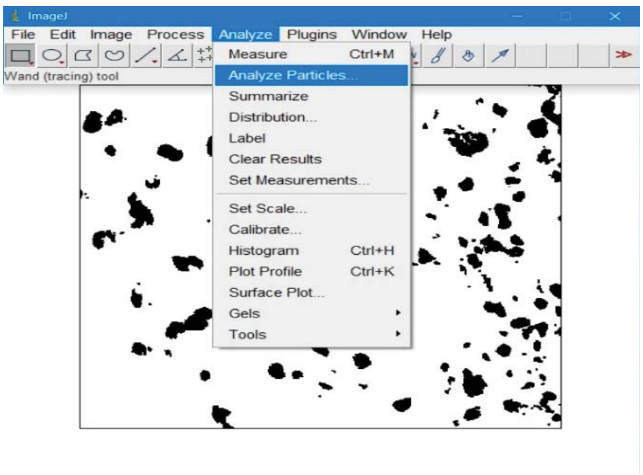

Fig. 10. Step 6: Particle analysis for the region with only bubbles.

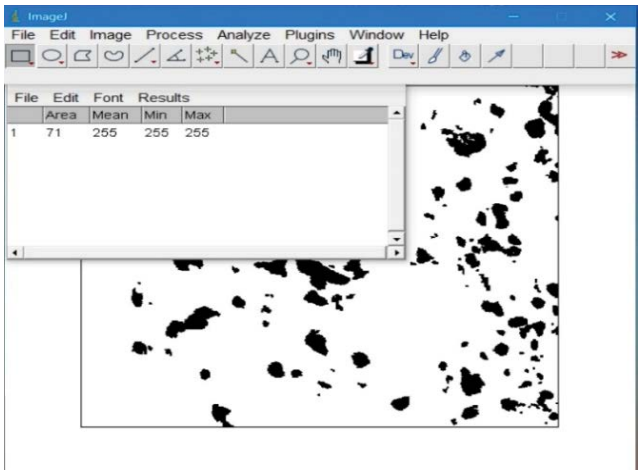

Fig. 11. Step 7: Number of particles after analysis.

respect to gas flow rate and projection depth of ejector. Finer bubbles have larger interfacial areas, thereby increasing gas holdup. Gas holdup functions as a concentration of the volume of bubbles that push the liquid out so that more gas occupies space [14]. This larger surface area also accelerates the gas exchange process into the solution. In Figs. 12 and 14 the 2 mm sparger produced the highest gas holdup of 0.146 at a projection depth of 27 cm and gas flow rate of 12.5 L/min. While the 3 mm sparger and 4 mm sparger produced 0.123 and 0.099, respectively.

4.3. Effect of liquid flow rate

The experiment was done by varying the liquid flow rate at constant gas flow rate. The influence of liquid flow rate on bubble diameter and bubble count was studied. As the flow rate increases the bubble count also increases in accordance with velocity and the bubble diameter decreases as flow rate increases [8]. As shown in Fig. 20 the results are found to be increasing gas hold up and gas–liquid interfacial area at higher liquid flow rates [15]. Figs. 24–27 show

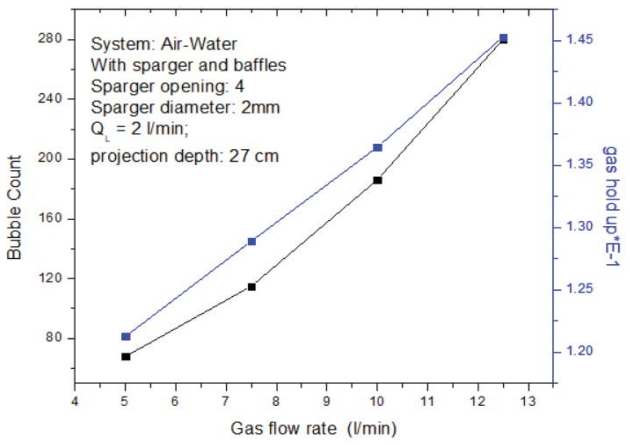

Fig. 12. Effect of gas flow rate on bubble count and gas holdup.

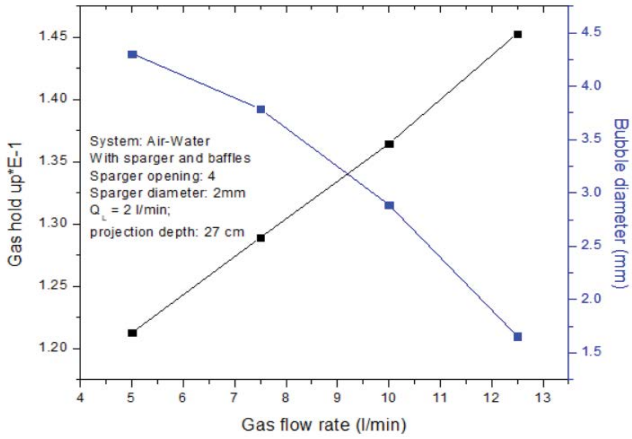

Fig. 13. Effect of gas flow rate on bubble count and $k_L a$.

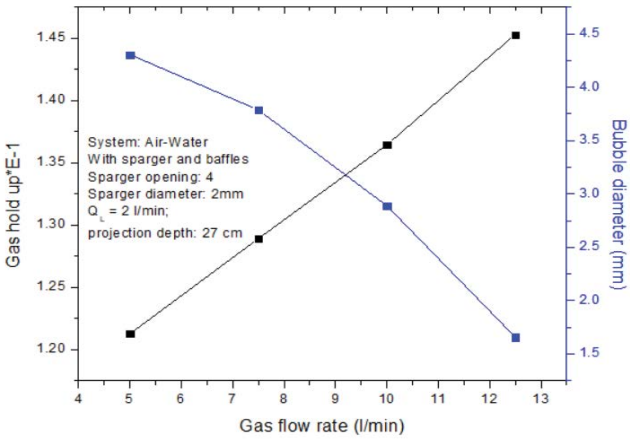

Fig. 14. Effect of gas flow rate on gas holdup and bubble diameter.

the bubble analysis (grey scale and threshold view) done using ImageJ software to find the average bubble diameter and approximate bubble count [23–27].

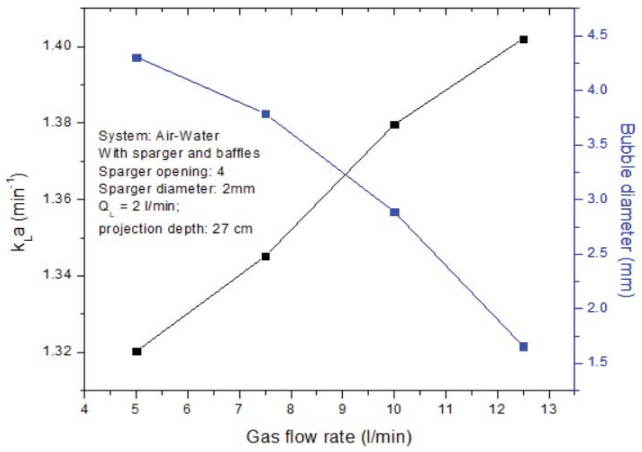

Fig. 15. Effect of gas flow rate on bubble diameter and k_La.

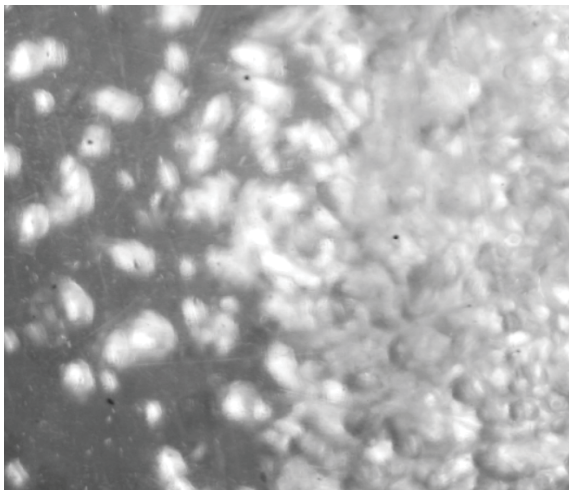

Fig. 16. Gas flow rate: 5 L/min; liquid flow rate: 2 L/min; projection depth: 27 cm; sparger diameter: 2 mm; sparger opening: 4 (grey scale).

Fig. 17. Gas flow rate: 5 L/min; liquid flow rate: 2 L/min; projection depth: 27 cm; sparger diameter: 2 mm; sparger opening: 4 (threshold view).

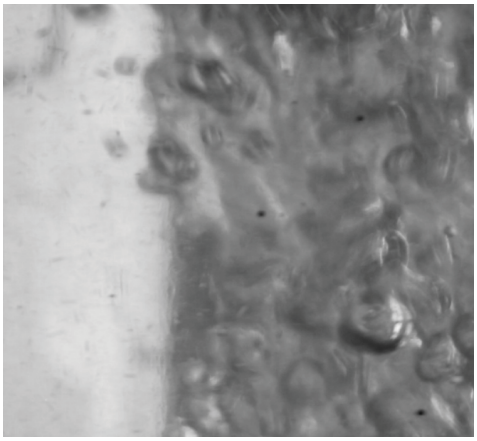

Fig. 18. Gas flow rate: 12.5 L/min; liquid flow rate: 2 L/min; projection depth: 27 cm; sparger diameter: 2 mm; sparger opening: 4 (grey scale).

Fig. 19. Gas flow rate: 12.5 L/min; liquid flow rate: 2 L/min; projection depth: 27 cm; sparger diameter: 2 mm; sparger opening: 4 (threshold view).

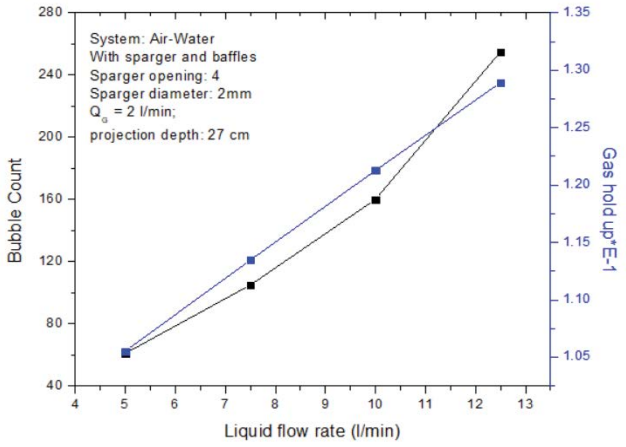

Fig. 20. Effect of liquid flow rate on bubble count and gas holdup.

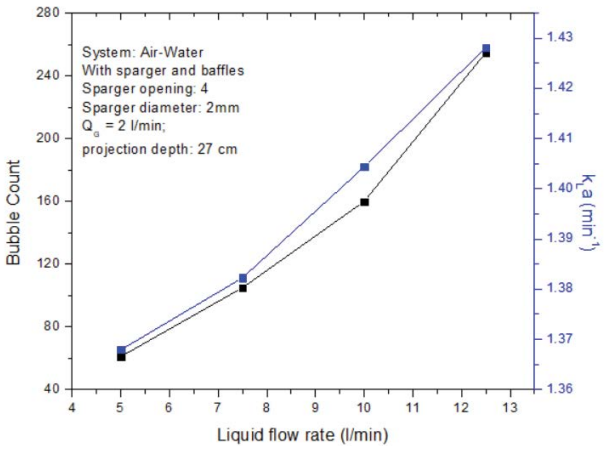

Fig. 21. Effect of liquid flow rate on bubble count and k_La.

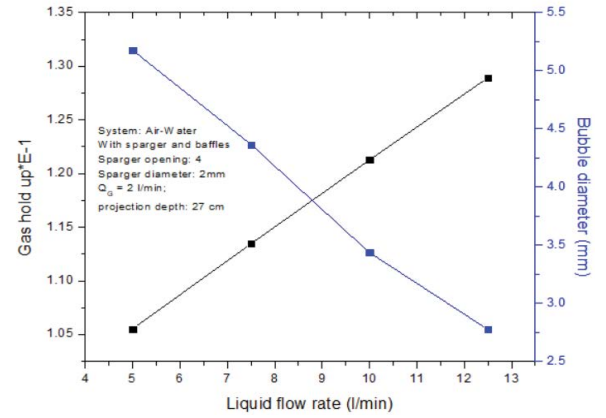

Fig. 22. Effect of liquid flow rate on bubble diameter and gas holdup.

4.4. Overall mass transfer coefficient and gas holdup variation with sparger geometry

In Figs. 21 and 23, the k_La associated with 2 mm sparger increases with respect to increase in liquid flow rate at projection depth of 27 cm at a constant gas flow rate of 2 L/min. Due to change in flow regime there is a considerable drop in k_La value while varying the liquid flow rate from 5–12.5 L/min. The 2 mm sparger produced the largest k_La of 1.428 min^{-1} at a projection depth of 27 cm and liquid flow rate of 12.5 L/min,while the 3 mm sparger and 4 mm sparger produced 1.378 and 1.353 min^{-1}, respectively. In Figs. 20 and 22, the 2 mm sparger produced the highest gas holdup of 0.146 at a projection depth of 27 cm and gas flow rate of 12.5 L/min. While the 3 mm sparger and 4 mm sparger produced 0.123 and 0.107, respectively for the above said conditions. Figs. 24–27 shows the bubble analysis (grey scale and threshold view) done using ImageJ software to find the average bubble diameter and approximate bubble count [23–27].

4.5. Effect of sparger

The sparger used definitely determines the bubble sizes observed in the column. Small orifice diameter plates

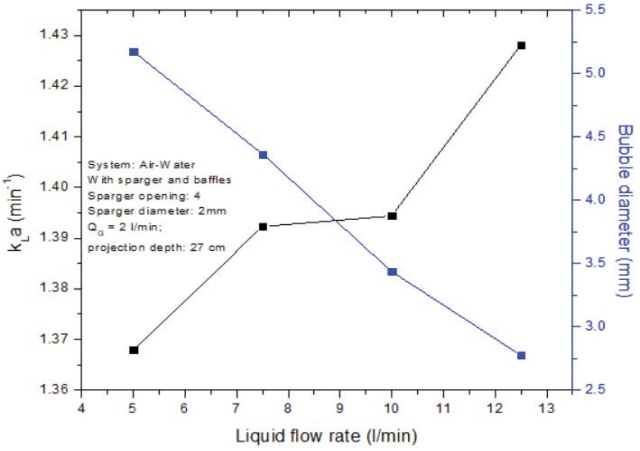

Fig. 23. Effect of liquid flow rate on bubble diameter and k_La.

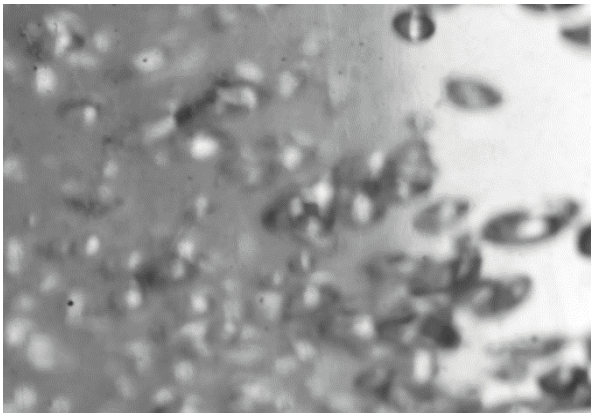

Fig. 24. Liquid flow rate: 5 L/min; gas flow rate: 2 L/min; projection depth: 27 cm; sparger diameter: 2mm; sparger opening: 4 (grey scale).

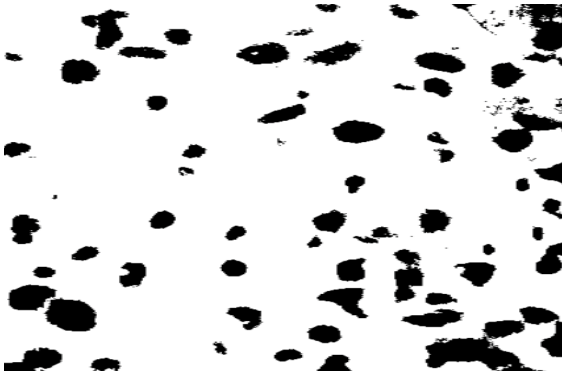

Fig. 25. Liquid flow rate: 5 L/min; gas flow rate: 2 L/min; projection depth: 27 cm; sparger diameter: 2mm; sparger opening: 4 (threshold view).

enable the formation of smaller sized bubbles and greater the gas hold up [18–22]. The experimental results showed that, the greater water flow rate, the greater the water pressure. This phenomenon is consistent with Henry's

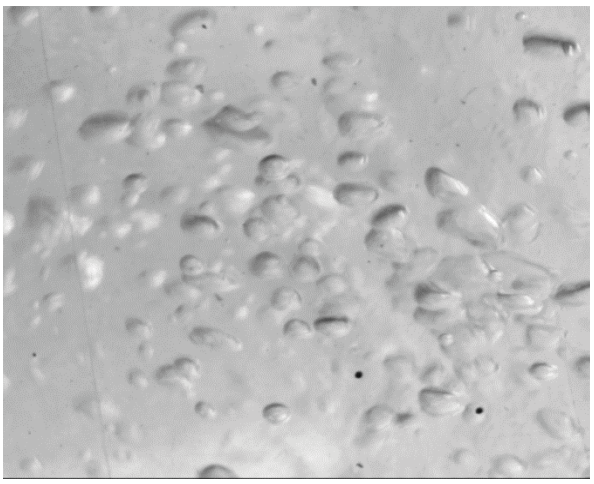

Fig. 26. Liquid flow rate: 12.5 L/min; gas flow rate: 2 L/min; projection depth: 27 cm; sparger diameter: 2mm; sparger opening: 4 (grey scale).

Fig. 27. Liquid flow rate: 12.5 L/min; gas flow rate: 2 L/min; projection depth: 27 cm; sparger diameter: 2mm; sparger opening: 4 (threshold view).

Law, which indicates that the increased pressure from the sparger allows greater dissolution of gases into the water [12]. In this investigation, the 2 mm sparger had the lowest water flow rate but produced the highest water pressure. In contrast, even though the 3 and 4 mm sparger had the highest water flow rate, it could not produce as much pressure as the 2 mm sparger. In Fig. 28, the 2 mm sparger shows that, the smaller the air flow rate that is regulated and the greater the difference in the water flow rate, the smaller the bubbles and more whiter or the water. The increasingly milky quality of the water indicates the presence of finer bubbles in large quantities [13]. Thus, the 2 mm sparger combines the largest water flow rate and the smallest airflow rate in producing finer bubbles.

4.6. Effect of baffles

When internal barriers like baffles are placed as obstacles inside the flow field, large bubbles break into smaller

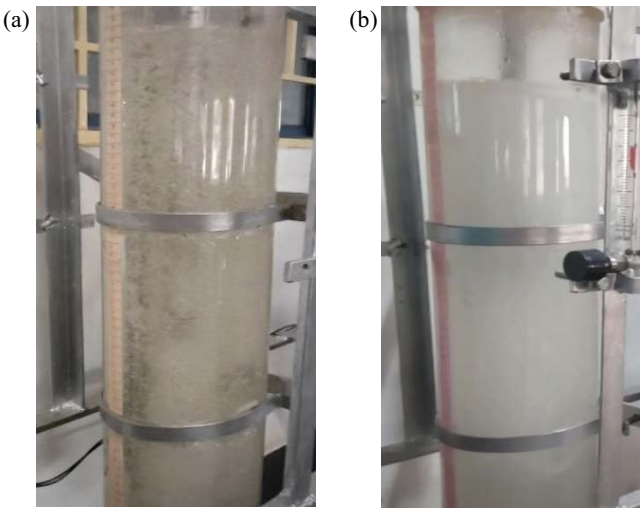

Fig. 28. Photo of reactor with 2 mm sparger (a) at liquid flow rate of 5 L/min and (b) at liquid flow rate of 12.5 L/min (milkier) with constant gas flow rate of 2 L/min in both (a) and (b).

ones, ensuring that the interfacial area between the dispersed gas phase and the continuous liquid phase remains large. Therefore, the introduction of non-circular baffles in our reactor enhanced the gas hold up, interfacial area and hence k_La [17]. The effect of baffles on gas hold up and k_La for various gas and liquid flow rate at 27 cm projection depth and 2 mm sparger is shown in Figs. 12 and 20.

We could understand that at 12.5 L/min of gas flow rate, the presence of non-circular baffles in the reactor registers the maximum k_La value of 1.402 min^{-1} when compared to the reactor without baffles of 1.230 min^{-1}. Also, at 12.5 L/min of liquid flow rate, the presence of non-circular baffles in the reactor registers the maximum k_La value of 1.428 min^{-1} when compared to the reactor without baffles of 1.185 min^{-1}. The reason is that gas bubbles are more held with increasing area under the baffle plates.

5. Conclusion

Based on the results of our study, the following conclusions are made.

- In our newly developed jet loop reactor, the investigation of bubble diameter and bubble count was successfully carried out by varying the operating and geometrical variables such as liquid and gas flow rates, sparger openings, and sparger diameter. The maximum bubble count of 280, minimum bubble size of 1.65 mm, and maximum mass transfer coefficient of 1.428 min^{-1} were observed at a liquid and gas flow rate of 12.5 L/min, sparger openings and diameter of 4 and 2 mm, respectively.
- The bubble count shows an increasing trend when we increased gas and liquid flow rates. From the graphical models, we strongly conclude that the values of overall mass transfer coefficient and gas holdup increases with increasing bubble count.
- In General, the bubble diameter shows a decreasing trend while increasing gas and liquid flow rates. The effect of

gas flow rate was more pronounced than that of liquid flow rate throughout our study. Thus when the bubble diameter was minimum, eventually the increasing cross-sectional area of the bubble leads to higher values of overall mass transfer coefficient and gas holdup.

References

[1] H. Blenke, Effect of liquid height on hydrodynamic characteristics of an external loop airlift reactor, Adv. Biochem. Eng., 13 (1979) 121–214.
[2] K.Tebel, H.P. Zehner, Fluid dynamic description of jet loop reactors in multi-phase operations, Chem. Eng. Technol., 12 (1989) 274–280.
[3] H.J. Warnecke, J. Prüss, H. Langemann, On a mathematical model for loop reactors-I. Residence time distribution, moments and eigenvalues, Chem. Eng. Sci., 40 (1985) 2321–2326.
[4] K. Bohner, H. Blenke, Verfahrenstechnik, loop reactors, Chem. Ing. Tech., 44 (1972) 373–373.
[5] A. Kulkarni, Y.T. Shah, Gas phase dispersion in a downflow bubble column, Chem. Eng. Commun., 28 (1984) 311–326.
[6] M. Velan, T.K. Ramanujam, Gas liquid mass transfer in a down flow jet loop reactor, Chem. Eng. Sci., 47 (1992) 2871–2876.
[7] N. Dutta, K. Raghavan, Mass transfer and hydrodynamic characteristics of loop reactors with down flow liquid jet ejector, Chem. Eng. J., 36 (1987) 111–121.
[8] M. Velan, T. Ramanujam, Hydrodynamics in down flow jet loop reactor, Can. J. Chem. Eng., 69 (1991) 1257–1261.
[9] S.M. Wagh, K.V. Koranne, R.B. Mankar, R.L. Sonolikaret, Gas holdup in a two-phase reversed flow jet loop reactor, Can. J. Chem. Eng., 88 (2010) 793–800.
[10] A.M. Jamshidi, M. Sohrabi, F. Vahabzadeh, B. Bonakdarpour, Hydrodynamic and mass transfer characterization of a down flow jet loop bioreactor, Biochem. Eng. J., 8 (2001) 241–250.
[11] L. Medic, A. Cehovin, T. Koloiui, A. Pavko, Volumetric gas–liquid mass coefficients in a rectangular bubble column with a rubber aeration pad, Chem. Eng. J., 41 (1989) B51–B54.
[12] M. Benjamin, D. Lawler, Water Quality Engineering: Physical/Chemical Treatment Processes, Wiley Publications, New Jersey, 2013.
[13] A. Agarwal, W.J. Ng, Y. Liu, Principle and applications of micro bubble and nano bubble technology for water treatment, Chemosphere, 84 (2011) 1175–1180.
[14] Y. Gao, D. Hong, H.Y. Cheng, L. Wang, X. Li, Gas holdup and liquid velocity distributions in the up flow jet-loop reactor, Chem. Eng. Res. Des., 136 (2018) 94–104.
[15] M. Millies, D. Mewes, Calculation of circulating flows in bubble columns, Chem. Eng. Sci., 50 (1995) 2093–2106.
[16] M. Zhao, K. Niranjan, J.F. Davidson, Mass transfer to viscous liquids in bubble columns and air-lift reactors: influence of baffles, Chem. Eng. Sci., 49 (1994) 2359–2369.
[17] F. Yamashita, Effect of liquid depth, column inclination and baffle plates on gas holdup in bubble columns, J. Chem. Eng. Jpn., 18 (1985) 349–363.
[18] X. Luo, D.J. Lee, R. Lau, G. Yang, L.S. Fan, Maximum stable bubble size and gas holdup in high-pressure slurry bubble columns, AlChE J., 45 (1999) 665–680.
[19] M. Bouaifi, G. Hebrard, D. Bastoul, M. Roustan, A comparative study of gas holdup, bubble size, interfacial area and mass transfer coefficients in stirred gas–liquid reactors and bubble columns, Chem. Eng. Process. Process Intensif., 40 (2001) 97–111.
[20] A. Schumpe, G. Grund, The gas disengagement technique for studying gas holdup structure in bubble columns, Can. J. Chem. Eng., 64 (1986) 891–896.
[21] C.L. Hyndman, F. Larachi, C. Guy, Understanding gas-phase hydro-dynamics in bubble columns: a convective model based on kinetic theory, Chem. Eng. Sci., 52 (1997) 63–77.
[22] A. Mandal, Characterization of gas–liquid parameters in a down-flow jet loop bubble column, Braz. J. Chem. Eng., 27 (2010) 253–264.
[23] M.D. Abràmoff, P.J. Magalhães, S.J. Ram, Image processing with ImageJ, Biophotonics Int., 11 (2004) 36–42.
[24] W.S. Rasband, ImageJ, US National Institutes of Health, Bethesda, Maryland, USA, 2011.
[25] C.A. Schneider, W.S. Rasband, K.W. Eliceiri, NIH Image to ImageJ: 25 Years of Image Analysis. Nature Methods, ImageJ, US National Institutes of Health, Bethesda, MD, USA, 2012, pp. 671–675.
[26] J. Behin, N. Farhadian, Residence time distribution measurements in a two dimensional rectangular airlift reactor by digital image processing, Exp. Therm. Fluid Sci., 51 (2013) 244–250.
[27] S.M. Hartig, Basic image analysis and manipulation in ImageJ, Curr. Protocol. Mol. Biol., 102 (2013) 14.15.1–14.15.12, doi: 10.1002/0471142727.mb1415s102.
[28] J. Behin, N. Farhadian, Digital image processing technique to investigate the hydrodynamics of an airlift reactor with double downcomer, Chem. Eng. Technol., 12 (2015) 2207–2216.
[29] A.E. Carpenter, T.R. Jones, M.R. Lamprecht, C. Clarke, I.H. Kang, O. Friman, D.A. Guertin, J.H. Chang, R.A. Lindquist, J. Moffat, P. Golland, D.M. Sabatini, CellProfiler: image analysis software for identifying and quantifying cell phenotypes, Genome Biol., 7 (2006) R100, doi: 10.1186/gb-2006-7-10-r100.
[30] N. Farhadian, J. Behin, A. Parvareh, Residence time distribution in an internal loop airlift reactor: CFD simulation versus digital image processing measurement, Comput. Fluids, 167 (2018) 221–228.